

Hysteresis of dynamos in rotating spherical shell convection

F. Feudel,^{1,*} L. S. Tuckerman,² M. Zaks,¹ and R. Hollerbach³

¹*Institut für Physik und Astronomie, Universität Potsdam, Karl-Liebknecht-Straße 24/25, 14476 Potsdam, Germany*

²*Laboratoire de Physique et Mécanique des Milieux Hétérogènes, CNRS, ESPCI Paris, PSL Research University, Sorbonne Université, Université Paris Diderot, 10 Rue Vauquelin, 75005 Paris, France*

³*Department of Applied Mathematics, University of Leeds, Woodhouse Lane, Leeds LS2 9JT, United Kingdom*

(Received 18 November 2016; published 16 May 2017)

Bifurcations of dynamos in rotating and buoyancy-driven spherical Rayleigh-Bénard convection in an electrically conducting fluid are investigated numerically. Both nonmagnetic and magnetic solution branches comprised of rotating waves are traced by path-following techniques, and their bifurcations and interconnections for different Ekman numbers are determined. In particular, the question of whether the dynamo branches bifurcate super- or sub-critically and whether a direct link to the primary pure convective states exists is answered.

DOI: [10.1103/PhysRevFluids.2.053902](https://doi.org/10.1103/PhysRevFluids.2.053902)

I. INTRODUCTION

It is generally accepted that dynamo action is responsible for the existence of large-scale magnetic fields in diverse astrophysical objects [1–3]; examples are found in the outer core of the earth or in the convection zone of the sun. A dynamo arises if an electrically conducting fluid flows in such a way that electromagnetic induction can maintain and enhance a magnetic field.

We study the idealized model consisting of an electrically conducting fluid in a rotating spherical shell that is buoyancy driven by a radial temperature gradient in the presence of a radially directed gravity field. This is one of the classical models of the earth's dynamo, which has been numerically proven to be able to generate and maintain a global magnetic field [4–12]. Depending on the parameter values, the dynamo may operate in different regimes [13–15].

One aspect that is believed to be important in the earth's core is the distinction between so-called weak- and strong-field dynamos. Weak-field dynamos are those for which the Lorentz force is only changing the fluid flow relatively little in comparison to the nonmagnetic regime, whereas strong-field dynamos are those for which the Lorentz force switches the entire system to a completely different solution branch [16,17]. Multiple solution branches like this are believed to arise in rapidly rotating systems due to different ways in which the Taylor-Proudman constraint can be broken; see, for example, the reviews in Refs. [3,18,19].

An almost inevitable consequence of having such multiple solution branches is that the system can become vulnerable both to runaway field growth, where it suddenly switches from the weak to the strong branch, and to a so-called dynamo catastrophe, in which the entire dynamo process suddenly switches off. This latter event can occur when the strong-field branch is so strongly subcritical that it exists for Rayleigh numbers below the initial onset of the weak-field branch and possibly even below the initial onset of any convection at all. See, for example, [20,21] where externally imposed fields were used to study the resulting extreme sensitivity of some of these solution branches.

A proper understanding of these multiple solution branches and where in parameter space either the runaway field growth or the dynamo catastrophe is likely to occur would therefore require mapping out the entire bifurcation structure of all branches, ideally even including unstable solutions connecting different branches. The work presented here is a step in this direction. We

*Corresponding author: ffeudel@uni-potsdam.de

apply path-following techniques to the magnetohydrodynamic (MHD) equations that allow us to compute branches of stationary and rotating wave solutions more systematically. In addition to the time-asymptotic attractors, unstable solutions can also be determined, which helps to elucidate the bifurcation structure.

Although we are not able to reach rotation rates so rapid that distinct weak- and strong-field branches emerge, the branches we obtain already exhibit at least some degree of subcritical behavior, indicating that the bifurcation diagrams are remarkably rich even at modest rotation rates and that path-following techniques will be crucial in mapping out the full sequence of bifurcations throughout the entire parameter space. Path-following techniques have already been applied to nonmagnetic spherical shell convection in different parameter regimes; see, e.g., [22–26].

A benchmark [27,28] dynamo solution for prescribed parameters and initial condition is the starting point for this work. In the benchmark, a rotating wave (RW) with a fourfold symmetry, which corresponds to the cyclic Z_4 group, is formed as the time-asymptotic magnetic solution. Starting from this solution, the stable branch of the dynamo can in principle be obtained by simulations via changing the Rayleigh number in small steps. However, there exists a lowest critical Rayleigh number at which the dynamo disappears at a finite amplitude, a feature that supports the conjecture that it originates in a saddle-node bifurcation. The question of whether these dynamos bifurcate sub- or supercritically from the primary pure convective states is of general interest in the literature [29,30]. Here we address this question for the benchmark situation corresponding to an Ekman number of $\text{Ek} = 10^{-3}$.

Multistability is commonly observed in hydrodynamic configurations, such as convectively driven rotating fluid systems. This has been demonstrated for the nonmagnetic spherical shell convection in Refs. [25,31] and we extend these investigations to dynamos in this work. Multistability of dynamos has been found hitherto by Simitev and Busse [32] and by Morin [33]. Depending on the control parameters, there generally exists a large number of qualitatively different solution branches, but only a few of them are stable and hence observable.

We present the equations and numerical methods in Sec. II. Starting from the benchmark parameters, Sec. III shows that, in addition to the benchmark solution with a Z_4 cyclic symmetry, two other dynamo branches with Z_5 and Z_3 symmetry appear to be stable over a finite interval of the Rayleigh number. In Sec. IV we discuss the bifurcation-theoretic origin of dynamo solutions at a nearby Ekman number at which a codimension-2 bifurcation generates two convective RW branches. In Sec. V we compute the magnetic solution branches for different Ekman numbers and determine their stability ranges. Finally, Sec. VI presents some details concerning the codimension-2 bifurcation to convective RWs.

II. GOVERNING EQUATIONS AND NUMERICAL METHODS

We study Rayleigh-Bénard convection of an electrically conducting fluid in a spherical shell rotating with a constant angular velocity $\boldsymbol{\Omega} = \Omega \mathbf{e}_z$. The fluid is heated from within by imposing a constant temperature difference ΔT between inner and outer spheres of radius r_i and r_o and is buoyancy driven by the action of a radial directed gravity force. Rescaling the length by the gap size d , time by the viscous time d^2/ν (ν is the kinematic viscosity), temperature by ΔT , pressure by $\rho_0 \nu \Omega$ (ρ_0 is the reference density), and the magnetic field by $\sqrt{\rho_0 \mu \eta \Omega}$ (μ is the magnetic permeability and η is the magnetic diffusivity), the MHD equations can be written in nondimensional form as

$$\text{Ek} \left[\frac{\partial \mathbf{u}}{\partial t} + \mathbf{u} \cdot \nabla \mathbf{u} - \nabla^2 \mathbf{u} \right] = -\nabla p - 2\mathbf{e}_z \times \mathbf{u} + \text{Ra} T \frac{\mathbf{r}}{r_0} + \frac{1}{\text{Pm}} (\nabla \times \mathbf{B}) \times \mathbf{B}, \quad (1a)$$

$$\frac{\partial \mathbf{B}}{\partial t} - \nabla \times (\mathbf{u} \times \mathbf{B}) = \frac{1}{\text{Pm}} \nabla^2 \mathbf{B}, \quad (1b)$$

$$\frac{\partial T}{\partial t} + \mathbf{u} \cdot \nabla T = \frac{1}{\text{Pr}} \nabla^2 T, \quad (1c)$$

$$\nabla \cdot \mathbf{u} = 0, \quad \nabla \cdot \mathbf{B} = 0. \quad (1d)$$

The nondimensional parameters in these equations

$$\text{Ek} = \frac{\nu}{d^2\Omega}, \quad \text{Ra} = \frac{\alpha\Delta T g_o d}{\Omega\nu}, \quad \text{Pr} = \frac{\nu}{\kappa}, \quad \text{Pm} = \frac{\nu}{\eta}, \quad \chi = \frac{r_i}{r_o} \quad (2)$$

are the Ekman number, a modified Rayleigh number (α is the thermal expansion coefficient), the Prandtl number (κ is the thermal diffusivity), the magnetic Prandtl number (η is the magnetic diffusivity) and the radius ratio of the spherical shell. We imposed rigid and thermally perfectly conducting boundary conditions, corresponding to

$$\mathbf{u} = 0 \quad \text{at } r = r_i, r_o, \quad (3a)$$

$$T = \begin{cases} 1 & \text{at } r = r_i \\ 0 & \text{at } r = r_o, \end{cases} \quad (3b)$$

and electrically insulating boundary conditions for the current density $\mathbf{j} = \nabla \times \mathbf{B}$,

$$\mathbf{e}_r \cdot \mathbf{j} = 0 \quad \text{at } r = r_i, r_o, \quad (4)$$

on the spherical surfaces (\mathbf{e}_r is the radial unit vector). This last equation provides the condition that the poloidal magnetic field can be extrapolated as a potential field into the insulating regions.

Following the benchmark study in Ref. [27], in this work we fix $\text{Pr} = 1$, $\text{Pm} = 5$, and the aspect ratio $\chi = 0.35$ ($r_o = 20/13$ and $r_i = 7/13$ so that $r_o - r_i = 1$). Here Ek and Ra are the remaining control parameters that will be varied in this study. We will use the kinetic and magnetic energy densities E_{kin} and E_{mag} , respectively, averaged over the volume V_s of the spherical shell

$$E_{\text{kin}} = \frac{1}{2V_s} \int_{V_s} \mathbf{u}^2 d^3r, \quad (5a)$$

$$E_{\text{mag}} = \frac{1}{2V_s \text{Ek} \text{Pm}} \int_{V_s} \mathbf{B}^2 d^3r, \quad (5b)$$

as well as a mixed quantity $E = E_{\text{kin}} + 0.25E_{\text{mag}}$ as global functions in our bifurcation diagrams. We choose the arbitrary weighting factor 0.25 in order to be able to present magnetic and pure convective solution branches in the same bifurcation diagram.

In our numerical treatment we extend the spectral code developed by Hollerbach [34] by implementing a Newton solver for stationary states and rotating waves in order to trace the dependence of the solution branches on the Rayleigh or Ekman number. The Newton solver uses Stokes preconditioning and the matrix-free biconjugate gradient stabilized (BiCGSTAB) algorithm [35] to solve the linear systems. This approach of using a standard time-stepping code and adapting it to carry out Newton's method was originally developed by Mamun and Tuckerman [36] and has been successfully applied to a variety of fluid problems [22,25,37]. See these references for more a detailed exposition.

Our numerical spectral discretization uses 36 wave numbers for the spherical harmonics in both the latitudinal and longitudinal directions and up to a degree of 36 Chebyshev polynomials in the radial direction. Below we will use the term mode number m in order to refer to the corresponding longitudinal components in the spectral decomposition of the variables.

III. DYNAMOS AT THE BENCHMARK ROTATION RATE

As stated in Sec. II, the gap size and thermal and magnetic Prandtl numbers have been set to the benchmark values. The benchmark was carried out for the special Ekman and Rayleigh numbers of $\text{Ek} = 0.001$ and $\text{Ra} = 100$ (cf. in Refs. [27,28]). Starting from the initial conditions described there,

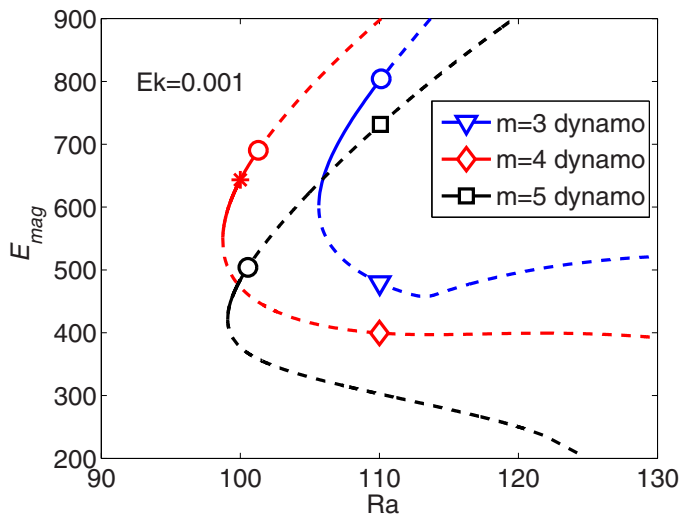


FIG. 1. Magnetic RWs for $Ek = 0.001$ of the $m = 3, 4,$ and 5 dynamos. The star marks the benchmark example at the $m = 4$ branch and open circles mark supercritical Hopf bifurcations. Solid (dashed) lines denote stable (unstable) solutions.

i.e., a quiescent fluid, a temperature field with fourfold azimuthal symmetry and an azimuthally homogeneous magnetic field, a dynamo with a dominant $m = 4$ mode evolves as a time-asymptotic solution. The generated pattern drifts along the azimuthal direction as a rotating wave, i.e., without changing its shape. One motivation for this work is to study the origin of this solution branch and to search for further qualitatively different dynamos. Fixing the Ekman number to $Ek = 0.001$, varying the Rayleigh number, and using different initial conditions, we found empirically two other dynamo branches with dominant $m = 3$ and $m = 5$ modes. These solutions are apparently stable because they were obtained as time-asymptotic solutions by simulations. Taking them as initial conditions for the path-following procedure, the corresponding solution branches, stable and unstable, can be traced. The resulting bifurcation diagram of the magnetic-field branches is presented in Fig. 1.

Imposing small perturbations and computing growth rates along the branches and then interpolating in the vicinity of the expected critical points, the stability regions of the magnetic RWs can be accurately determined. Surprisingly, in particular for the $m = 4$ and $m = 5$ solutions, they are rather narrow. Note that if the branches are traced by simulations ramping the Rayleigh number in small steps, a very long simulation time is required to reach the asymptotic states. The growth rates of the unstable modes are very small and hence the stability interval is in practice often overestimated. This demonstrates the advantage of our approach of first fixing the RWs by the Newton method and then calculating the leading eigenvalue by interpolating between the growth rates along the computed branches.

As can be seen in Fig. 1, the three magnetic RWs appear and attain stability via saddle-node bifurcations. At higher Rayleigh numbers, each of them in turn loses stability via a supercritical Hopf bifurcation. Hopf bifurcations of RWs in $SO(2)$ equivariant systems generate modulated RWs (MRWs) (see also [38,39]), which are simply time-periodic solutions in coordinate frames moving with the speed of the corresponding wave. In addition, they possess a spatiotemporal symmetry that can be classified by methods of equivariant bifurcation theory [40]. In Ref. [31] we classified the MRWs that bifurcate from the pure convective RWs for $Ek = 0.001$, the same value as studied here. The same convective MRWs exist and are stable for the present problem, but for more details the reader is referred to [31]. The classification of the spatiotemporal symmetry for the magnetic MRWs that appear is straightforward, but is outside the scope of this work.

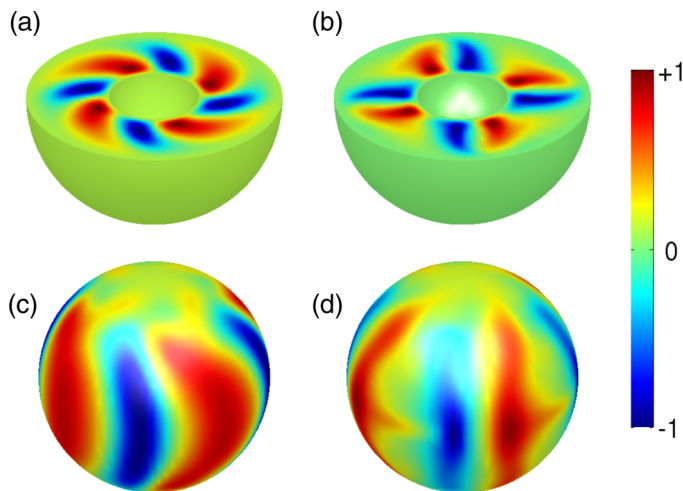


FIG. 2. Contour plots of the radial velocity for the nonmagnetic solution (a) in the equatorial plane and (c) in the middle of the spherical gap at $Ek = 0.001$ and $Ra = 100$. (b) and (d) Same for the dynamo solution. In each plot the color is normalized to the maximum (red) and minimum (blue) of the presented field component.

Corresponding to each magnetic branch in Fig. 1 there exists a pure convective branch with the same cyclic symmetry, not shown here but extensively discussed in Ref. [31] (in particular cf. Fig. 3 contained therein). Since each of the considered magnetic branches is stable over a certain interval of Ra together with the convective branch of the same symmetry, a high degree of multistability can be observed.

There is still the question of whether all lower magnetic branches are linked to the primary convective branches via subcritical bifurcations. We did not detect any magnetic instability along the stable portions of the convective branches; they become unstable via secondary nonmagnetic Hopf bifurcations. For $m = 4$ we were able to compute the whole magnetic branch and found the link to its primary convective branch at $Ra = 139.1$. The convective branch is already unstable at this Rayleigh number. Since the path-following procedure for the low Ekman number of the benchmark is very time consuming, we will discuss the question how the dynamo solutions are generated and how they are stabilized in more detail for slightly higher Ekman numbers in the following sections.

In order to give an impression of the convection patterns and to demonstrate the feedback of the Lorentz force on the flow, Fig. 2 shows contour plots of the radial velocity both for the nonmagnetic solutions [Figs. 2(a) and 2(c)] and for the dynamo solutions [Figs. 2(b) and 2(d)], in the equatorial plane and in the middle of the spherical gap, respectively. The bright color (red) corresponds to strong positive radial velocities and can be interpreted as regions of warm ascending fluid and dark color (blue) marks regions of cold descending fluid. In Figs. 2(b) and 2(d) one recognizes the typical structure of convection rolls oriented along the rotation axis. The spiral structure of the nonmagnetic convection rolls [Figs. 2(a) and 2(c)] is squeezed by the Lorentz force, leading to rolls in the magnetic situation [Figs. 2(b) and 2(d)], which are less extended along the azimuthal direction. Since the Lorentz force does not deform the flow substantially (the axial Z_4 symmetry is retained) the stable magnetic solutions can be classified as weak-field dynamos [17].

IV. BIFURCATIONS OF MAGNETIC BRANCHES FROM CONVECTIVE BRANCHES

In the study in Ref. [25] we determined by means of a linear stability analysis that at $Ek \approx 0.00164$ two nonmagnetic RWs with $m = 3$ and $m = 4$ bifurcate simultaneously from the conductive base state. This degenerate situation, in which more than one mode is produced at a bifurcation, is also referred to as a mode interaction [40–42]. Since codimension-2 bifurcations have a strong impact

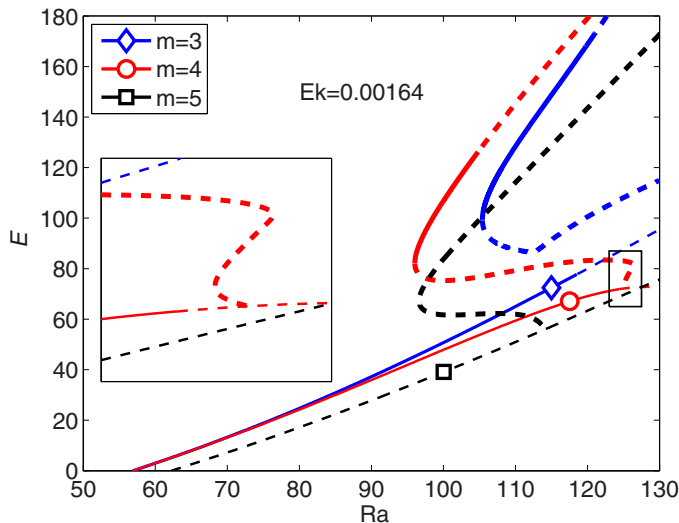


FIG. 3. Convective (primary) and magnetic (secondary) bifurcations of RWs for $Ek = 0.00164$. On the vertical axis, $E = E_{\text{kin}} + 0.25 E_{\text{mag}}$. Thick lines mark the dynamo branches. The inset shows a close-up of the $m = 4$ bifurcating magnetic branch.

on the surrounding parameter region, we carry out a more detailed study of the bifurcation scenario at this Ekman number.

Figure 3 shows both the primary bifurcations leading to the pure convective branches (thin lines) and the secondary bifurcations generating the dynamo branches (thick lines). In order to represent the convective and magnetic branches together in one figure the global function on the ordinate axis is chosen to be the sum of the kinetic and a quarter of the magnetic energy, $E = E_{\text{kin}} + 0.25 E_{\text{mag}}$.

The conductive state becomes unstable at the double Hopf bifurcation of the $m = 3$ and $m = 4$ modes at a critical Rayleigh number $Ra_{\text{dH}} = 56.87$, where two stable nonmagnetic RWs with cyclic symmetry Z_3 and Z_4 are created. The kinetic energy should vary linearly with Ra at a supercritical Hopf bifurcation and this is indeed the case. At Ra_{dH} , the two branches are tangent and form a cusp. Both branches are then destabilized by secondary supercritical Hopf bifurcations; the resulting unstable parts of the branches are drawn as dashed lines in Fig. 3. The attractors emerging beyond that point are convective MRWs, not depicted here. The next convective instabilities of the conducting state are the $m = 5$ mode, which appears at $Ra = 62.22$ and remains unstable for all Rayleigh numbers studied, and subsequently the $m = 2$ mode, which emerges at $Ra = 64.08$ and is not shown in Fig. 3.

Corresponding to each of the convective RWs presented in Fig. 3, we have found an associated magnetic branch with the same cyclic symmetry. Starting from the stable magnetic solutions at $Ek = 0.001$ described in the previous section, we increased the Ekman number to Ek_{dH} . Starting from these fields, both the stable and unstable magnetic branches, drawn as thick lines in the bifurcation diagram, could be traced as functions of the Rayleigh number by means of the path-following scheme.

The magnetic branches appear at their lowest Rayleigh number via saddle-node bifurcations similar to the situation at $Ek = 0.001$ in Fig. 1. We have traced the magnetic solutions back to their original bifurcations from the pure convective branches. Figure 3 shows the bifurcations at $Ra = 126.87$ for $m = 4$ and $Ra = 114.09$ for $m = 5$, at which these two dynamos are born. The connection between the $m = 3$ dynamo and its original convective counterpart is not captured in this figure. Unlike for $Ek = 0.001$ in Fig. 1, here both the convective and magnetic branches of the $m = 5$ mode are unstable for all Rayleigh numbers.

An essential feature of this configuration is that the bifurcations to magnetic branches occur at Rayleigh numbers at which the convective branches are already unstable. However, some of the

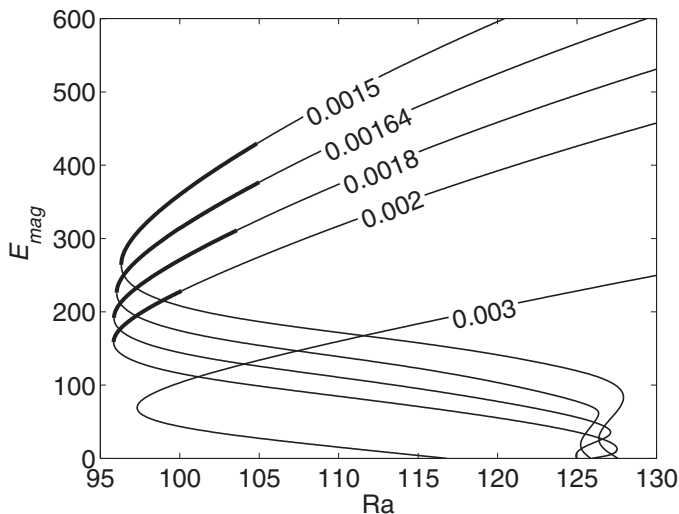


FIG. 4. The $m = 4$ dynamos for various Ekman numbers, which are labeled at the corresponding branches. Thick (thin) lines mark stable (unstable) solutions.

magnetic branches eventually are stabilized via turning points, as demonstrated in Fig. 3 for the $m = 4$ dynamo branch.

V. DYNAMO GENERATION FOR A VARIETY OF EKMAN NUMBERS

In this section we investigate how the $m = 3$ and $m = 4$ dynamos are influenced by the rotation rates for a variety of Ekman numbers around the codimension-2 point, $Ek = 0.00164$, discussed in the preceding section.

In Fig. 4 the $m = 4$ dynamo branches are depicted for five Ekman numbers between 0.003 and 0.0015. All of these branches are created via saddle-node bifurcations in a narrow range of Rayleigh numbers $95.8 < Ra < 97.4$, but not all of them have a stable portion.

For the lowest rotation rate $Ek = 0.003$, the magnetic branch bifurcates at $Ra = 116.8$ subcritically from the corresponding nonmagnetic convective states with the same cyclic symmetry. However, this primary convective state is already unstable, with two eigenvalues that have positive real parts. This situation and the others presented in Fig. 4 are qualitatively similar to the case extensively discussed in the preceding section ($Ek = 0.00164$); that is, the primary convective branches have already lost their stability via a Hopf bifurcation before the magnetic instability occurs. For smaller Ekman numbers ($Ek \leq 0.002$) the generated magnetic branches are stabilized at the final saddle-node bifurcations as shown, e.g., for the magnetic branch of the $m = 4$ mode in Fig. 3. At $Ek = 0.002$ the bifurcation creating the magnetic solution is supercritical, with an adjacent subsequent turning point, after which the magnetic solution has a single positive eigenvalue. This remaining positive eigenvalue changes sign at the final saddle-node bifurcation, which produces a stable dynamo.

For the smaller Ekman numbers in Fig. 4, $Ek = 0.0018, 0.00164, 0.0015$, the generation of the magnetic branches is more subtle. The bifurcations creating the magnetic branches are subcritical, leading to branches that have three eigenvalues with positive real parts, and two subsequent adjacent turning points stabilize the branches, so the third and final saddle-node bifurcation at $Ra \approx 95$ leads to stable dynamo solutions. Generally, we observe that under the increase of Ek (decrease of the rotation rate) the point of the Hopf bifurcation on the upper solution branch in Fig. 4 moves to the left and the stability interval for magnetic RWs gets shorter until it finally vanishes.

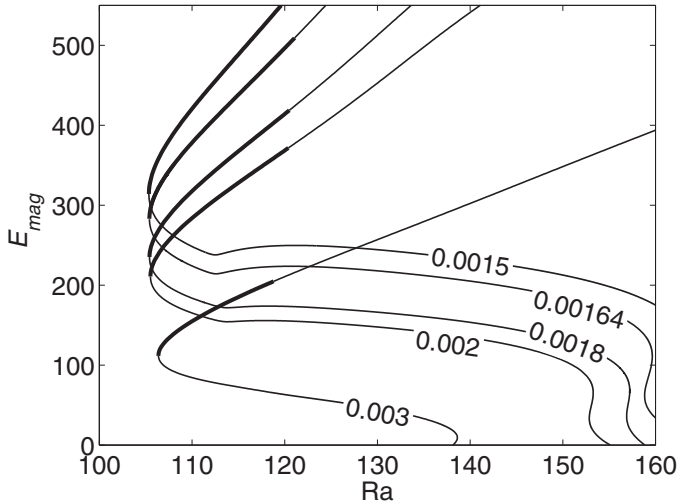


FIG. 5. The $m = 3$ dynamo branches for the same Ekman numbers as in Fig. 4.

The bifurcation scenario for the $m = 3$ magnetic solutions has been computed for the same Ekman numbers and is presented in Fig. 5. The magnetic branches appear again via saddle-node bifurcations at comparable Rayleigh numbers, but the bifurcations from the pure convective branches are shifted to higher Rayleigh numbers. The pure convective branches are all unstable at these points and a sequence of subsequent adjacent turning points ensures that the magnetic solutions are stabilized by the final saddle-node bifurcation. Although we did not compute these links explicitly in all cases, there are strong indications that all the magnetic branches bifurcate from the corresponding pure convective branches and the bifurcation points are shifted to higher Rayleigh numbers as the Ekman numbers (rotation rates) decrease (increase).

VI. CODIMENSION-2 BIFURCATION

Section IV described the bifurcation diagram for $\text{Ek}_{\text{dH}} = 0.00164$, at which two nonmagnetic RWs, one with $m = 3$ and one with $m = 4$, bifurcate from the conductive state at $\text{Ra}_{\text{dH}} = 56.87$ via a double Hopf bifurcation. Here we discuss this codimension-2 bifurcation in the framework of normal forms.

Both of the RW branches are stable at onset; this can be explained by the features of the double Hopf point that are in turn determined by the governing amplitude equations. The $\text{SO}(2)$ equivariant normal form for the complex amplitudes z_m and z_n of a double Hopf bifurcation up to third order (cf. [41,43]) is

$$\dot{z}_m = \lambda_m z_m - (\alpha_m |z_m|^2 + \beta_m |z_n|^2) z_m, \quad \dot{z}_n = \lambda_n z_n - (\beta_n |z_m|^2 + \alpha_n |z_n|^2) z_n, \quad (6)$$

where $\lambda = \sigma + i\omega$, α , and β are complex functions of Ra and Ek . The real parts of λ_m and λ_n simultaneously vanish at the critical values Ek_{dH} and Ra_{dH} . Numerical results indicate that in our example the product of real parts of α_m and α_n is positive. This allows us to discard in the normal form the quintic terms, which, in this situation, do not influence the topology of the bifurcation diagram (see also [43–45]).

Decomposing the complex modes in terms of amplitudes and phases $z = r e^{i\varphi}$, Eqs. (6) separate into four real equations

$$\dot{r}_m = \sigma_m r_m - (\alpha_m^R r_m^2 + \beta_m^R r_n^2) r_m, \quad \dot{r}_n = \sigma_n r_n - (\beta_n^R r_m^2 + \alpha_n^R r_n^2) r_n, \quad (7)$$

$$\dot{\phi}_m = \omega_m - (\alpha_m^I r_m^2 + \beta_m^I r_n^2), \quad \dot{\phi}_n = \omega_n - (\beta_n^I r_m^2 + \alpha_n^I r_n^2), \quad (8)$$

Eqs. (7) for the amplitudes and Eqs. (8) for the phases, where the upper indices R and I denote the real and imaginary parts of the complex coefficients α_m and β_m . Our numerical simulations show that both branches of rotating waves are born via supercritical Hopf bifurcations; they are observed in the parameter region where the respective growth rates σ_m and σ_n are positive. Hence α_m^R and α_n^R must also be positive and so the variables can be rescaled so that $\alpha_m^R = \alpha_n^R = 1$. Solutions with constant amplitudes (r_m, r_n) of Eqs. (7) are the pure modes

$$P_m = (\sqrt{\sigma_m}, 0), \quad P_n = (0, \sqrt{\sigma_n}), \quad (9)$$

which correspond to the two branches of rotating waves, and the mixed modes

$$P_{mn} = \left(\sqrt{\frac{\sigma_m - \beta_m^R \sigma_n}{1 - \beta_m^R \beta_n^R}}, \sqrt{\frac{\sigma_n - \beta_n^R \sigma_m}{1 - \beta_m^R \beta_n^R}} \right), \quad (10)$$

which correspond here to unstable modulated rotating waves. The branch P_m is stable for $\sigma_n < \beta_n^R \sigma_m$, whereas P_n is stable for $\sigma_m < \beta_m^R \sigma_n$. Thus, if

$$\beta_m^R \beta_n^R > 1, \quad (11)$$

then there exists a range $\beta_n^R > \sigma_n / \sigma_m > 1 / \beta_m^R$ over which both pure modes are stable, which has been shown to be the case by our numerical results. The basins of attraction of these stable branches are separated by the stable manifold of the mixed mode states, i.e., the modulated rotating waves. Equation (11) is a lower bound on the interaction coefficients between modes m and n . For the opposite situation, i.e., unfolding of the double Hopf with a stable mixed mode (modulated rotating wave) and unstable pure modes (rotating waves) see, e.g., [45] in the case of a driven flow in a cylinder.

Away from the codimension-2 point, the $m = 4$ branch bifurcates first for $\text{Ek} < \text{Ek}_{\text{dH}}$, while the $m = 3$ branch bifurcates first for $\text{Ek} > \text{Ek}_{\text{dH}}$; both branches exchange their stability at this point. In each case, the branch that bifurcates for higher Ra is at first unstable and is stabilized in a secondary bifurcation that produces the mixed-mode branch.

Although we have not computed the values of the normal form coefficients, we have deduced some relations between them that follow from the dynamics of the configuration we have studied.

VII. CONCLUSION

The purpose of this work has been to study the general solution structure of convective driven magnetic RWs in spherical shells over a wide range of Ekman numbers systematically by means of path-following techniques. Corresponding to the benchmark problem with $\text{Ek} = 0.001$, we have found three stable dynamo branches in the form of cyclically symmetric RWs with one dominant azimuthal mode, $m = 3, 4$, or 5 . All of them are subcritical in the sense that they first appear (at their lowest values of Rayleigh number) via saddle-node bifurcations.

We have studied in detail the bifurcations of both the pure convective and the magnetic solutions near the codimension-2 point at $\text{Ek} = 0.00164$. At the onset of convection, two nonmagnetic RWs bifurcate from the conductive state via a double Hopf bifurcation.

Another part of this work has been devoted to the dynamo generation in which both stable and unstable branches were computed for a variety of Ekman numbers. In the parameter range considered, it has been found that for each convective branch of the $m = 3, 4$, and 5 modes, a related

dynamo with the same symmetry exists. They appear via saddle-node bifurcations and their stability depends on the rotation rate. Both stable and unstable parts of the branches have been traced and, by means of this approach, explicit links to the primary pure convection branches have been computed. In this sense the dynamos bifurcate subcritically and are eventually stabilized over a subsequent number of turning points.

ACKNOWLEDGMENT

F.F. wishes to thank Edgar Knobloch for helpful discussions.

-
- [1] G. A. Glatzmaier, Numerical simulations of stellar convective dynamos. I. The model and method, *J. Comput. Phys.* **55**, 461 (1984).
 - [2] M. R. E. Proctor and A. D. Gilbert, *Lectures on Solar and Planetary Dynamos* (Cambridge University Press, Cambridge, 1994).
 - [3] G. Rüdiger and R. Hollerbach, *The Magnetic Universe: Geophysical and Astrophysical Dynamo Theory* (Wiley-VCH, Berlin, 2004).
 - [4] G. A. Glatzmaier and P. H. Roberts, A three-dimensional self-consistent computer simulation of a geomagnetic field reversal, *Nature (London)* **377**, 203 (1995).
 - [5] G. A. Glatzmaier and P. H. Roberts, A three-dimensional convective dynamo solution with rotating and finitely conducting inner core and mantle, *Phys. Earth Planet. Inter.* **91**, 63 (1995).
 - [6] W. Hirsching and F. H. Busse, Stationary and chaotic dynamos in rotating spherical shells, *Phys. Earth Planet. Inter.* **90**, 243 (1995).
 - [7] J. Wicht and F. H. Busse, Magnetohydrodynamic dynamos in rotating spherical shells, *Geophys. Astrophys. Fluid Dyn.* **86**, 103 (1997).
 - [8] U. R. Christenson and J. Wicht, in *Treatise on Geophysics*, edited by G. Schubert (Elsevier, Amsterdam, 2007), pp. 245–282.
 - [9] J. Wicht and A. Tilgner, Theory and modeling of planetary dynamos, *Space Sci. Rev.* **152**, 501 (2010).
 - [10] C. Jones, Planetary magnetic fields and fluid dynamos, *Annu. Rev. Fluid Mech.* **43**, 583 (2011).
 - [11] P. H. Roberts and E. M. King, On the genesis of the earth’s magnetism, *Rep. Prog. Phys.* **76**, 096801 (2013).
 - [12] J. Wicht, S. Stellmach, and H. Harder, in *Handbook of Geomathematics*, 2nd ed., edited by W. Freeden, M. Z. Nashed, and T. Sonar (Springer, Berlin, 2015), p. 779.
 - [13] U. Christensen, P. Olsen, and G. A. Glatzmaier, Numerical modeling of the geodynamo: A systematic parameter study, *Geophys. J.* **138**, 393 (1999).
 - [14] E. Grote, F. H. Busse, and A. Tilgner, Regular and chaotic spherical dynamos, *Phys. Earth Planet. Inter.* **117**, 259 (2000).
 - [15] R. Simitev and F. H. Busse, Prandtl-number dependence of convection-driven dynamos in rotating spherical fluid shells, *J. Fluid Mech.* **532**, 365 (2005).
 - [16] E. Dormy, Strong-field spherical dynamos, *J. Fluid Mech.* **789**, 500 (2016).
 - [17] D. W. Hughes and F. Cattaneo, Strong-field dynamo action in rapidly rotating convection with no inertia, *Phys. Rev. E* **93**, 061101(R) (2016).
 - [18] K.-K. Zhang and G. Schubert, Magnetohydrodynamics in rapidly rotating spherical systems, *Annu. Rev. Fluid Mech.* **32**, 409 (2000).
 - [19] E. Dormy, J.-P. Valet, and V. Courtillot, Numerical models of the geodynamo and observational constraints, *Geochem. Geophys. Geosyst.* **1**, 1037 (2000).
 - [20] K.-K. Zhang and D. Gubbins, Is the geodynamo process intrinsically unstable? *Geophys. J. Int.* **140**, F1 (2000).

- [21] K.-K. Zhang and D. Gubbins, Scale disparities and magnetohydrodynamics in the earth's core, *Philos. Trans. R. Soc. A* **358**, 899 (2000).
- [22] F. Feudel, K. Bergemann, L. S. Tuckerman, C. Egbers, B. Fütterer, M. Gellert, and R. Hollerbach, Convection patterns in a spherical fluid shell, *Phys. Rev. E* **83**, 046304 (2011).
- [23] K. Kimura, S.-I. Takehiro, and M. Yamada, Stability and bifurcation diagram of Boussinesq thermal convection in a moderately rotating spherical shell, *Phys. Fluids* **23**, 074101 (2011).
- [24] J. Sánchez, F. Garcia, and M. Net, Computation of azimuthal waves and their stability in thermal convection in rotating spherical shells with application to the study of a double-Hopf bifurcation, *Phys. Rev. E* **87**, 033014 (2013).
- [25] F. Feudel, L. S. Tuckerman, M. Gellert, and N. Seehafer, Bifurcations of rotating waves in rotating spherical shell convection, *Phys. Rev. E* **92**, 053015 (2015).
- [26] F. Garcia, M. Net, and J. Sánchez, Continuation and stability of convective modulated rotating waves in spherical shells, *Phys. Rev. E* **93**, 013119 (2016).
- [27] U. R. Christensen, J. Aubert, P. Cardin, E. Dormy, S. Gibbons, G. A. Glatzmaier, E. Grote, Y. Honkura, C. Jones, M. Kono, M. Matsushima, A. Sakuraba, F. Takahashi, A. Tilgner, J. Wicht, and K. Zhang, A numerical dynamo benchmark, *Phys. Earth Planet. Inter.* **128**, 25 (2001).
- [28] H. Matsui *et al.*, Performance benchmarks for a next generation numerical dynamo model, *Geochem. Geophys. Geosyst.* **17**, 1586 (2016).
- [29] D. Morin and E. Dormy, The dynamo bifurcation in rotating spherical shells, *Int. J. Mod. Phys. B* **23**, 5467 (2009).
- [30] E. Dormy, Stability and bifurcation of planetary dynamo models, *J. Fluid Mech.* **688**, 1 (2011).
- [31] F. Feudel, N. Seehafer, L. S. Tuckerman, and M. Gellert, Multistability in rotating spherical shell convection, *Phys. Rev. E* **87**, 023021 (2013).
- [32] R. Simitev and F. H. Busse, Bistability and hysteresis of dipolar dynamos generated by turbulent convection in rotating spherical shells, *Europhys. Lett.* **85**, 19001 (2009).
- [33] V. Morin, Multiple stability and influence of forcing modulation on dynamo action in a spherical shell, *Geophys. Astrophys. Fluid Dyn.* **104**, 153 (2010).
- [34] R. Hollerbach, A spectral solution of the magneto-convection equations in spherical geometry, *Int. J. Numer. Methods Fluids* **32**, 773 (2000).
- [35] H. van der Vorst, Bi-CGSTAB: A fast and smoothly converging variant of Bi-CG for the solution of nonsymmetric linear systems, *SIAM J. Sci. Stat. Comput.* **13**, 631 (1992).
- [36] C. K. Mamun and L. S. Tuckerman, Asymmetry and Hopf bifurcation in spherical Couette flow, *Phys. Fluids* **7**, 80 (1995).
- [37] K. Borońska and L. S. Tuckerman, Extreme multiplicity in cylindrical Rayleigh-Bénard convection. II. Bifurcation diagram and symmetry classification, *Phys. Rev. E* **81**, 036321 (2010).
- [38] D. Rand, Dynamics and symmetry. Predictions for modulated waves in rotating fluids, *Arch. Ration. Mech. Anal.* **79**, 1 (1982).
- [39] M. Renardy, Bifurcation from rotating waves, *Arch. Ration. Mech. Anal.* **79**, 49 (1982).
- [40] P. Chossat and R. Lauterbach, *Methods in Equivariant Bifurcations and Dynamical Systems* (World Scientific, Singapore, 2000).
- [41] M. Golubitsky, I. Stewart, and D. G. Schaeffer, *Singularities and Groups in Bifurcation Theory* (Springer, New York, 1988), Vol. II.
- [42] J. D. Crawford and E. Knobloch, Symmetry and symmetry breaking bifurcations in fluid dynamics, *Annu. Rev. Fluid Mech.* **23**, 341 (1991).
- [43] Y. A. Kuznetsov, *Elements of Applied Bifurcation Theory* (Springer, New York, 2004).
- [44] F. Marques, J. M. Lopez, and J. Shen, Mode interactions in an enclosed swirling flow: A double Hopf bifurcation between azimuthal wave numbers 0 and 2, *J. Fluid Mech.* **455**, 261 (2002).
- [45] J. M. Lopez and F. Marques, Mode competition between rotating waves in a swirling flow with reflection symmetry, *J. Fluid Mech.* **507**, 265 (2004).